Modeling of Flapping-Wing Rectifier Systems and Optimal Gait Analysis ⋆

Justin T. Blair * **Tetsuya Iwasaki** **

* *Department of Mechanical and Aerospace Engineering, University of Virginia, 122 Engineer's Way, Charlottesville, VA 22904 USA, e-mail: jtb8s@virginia.edu*
** *Department of Mechanical and Aerospace Engineering, University of California, 420 Westwood Plaza, Los Angeles, CA 90095 USA, e-mail: tiwasaki@ucla.edu*

Abstract: Flapping-wing rectifier systems are defined as systems which produce bulk locomotion through the interaction of periodic wing movement with a surrounding environment. A nonlinear model is developed featuring a 6 degree-of-freedom main body (position and orientation) and wing deformation. Each wing may move independently and is described as the motion of many discrete points in the body-fixed coordinate frame. The nonlinear model is approximated with a bilinear model through Taylor series, which is then used in an optimal gait analysis. Various wing shapes and optimality criteria are considered, such as the thrust to deflection ratio and the overall actuation effort to generate a variety of gaits.

Keywords: Optimal Control; Animal Locomotion; Motion Planning; Gait; Underwater vehicle.

1. INTRODUCTION

This is an extension of our previous paper (Blair and Iwasaki (2011)), wherein animal locomotion is viewed as mechanical rectification, in that the periodic motion of the animal's body (or "gait") produces a sustained thrust through interactions with the environment. The fundamental problem in animal locomotion is the determination of a gait for a given body (or mechanical system) that achieves a desired velocity. There may be many possible gaits that produce a desired velocity for a given system (for example a human may run, skip, or speed-walk), so an additional condition is needed, such as minimizing the energy cost of locomotion. The problem is further complicated by the possibility that an animal's body may be under-actuated.

Most existing optimal gait approaches generally search for local minima using fully nonlinear equations of motion, and the numerical solutions depend on initial conditions (i.e. parameterization and gridding (Chevallereau and Aoustin (2001); Saito et al. (2002); McIsaac and Ostrowski (2003)), basis function expansion (Cortes et al. (2001); Saidouni and Bessonnet (2003); Srinivasan and Ruina (2006)), and two-point boundary-value problems using calculus of variations (Ostrowski et al. (2000); Bessonnet et al. (2004); Hicks and Ito (2005))). In contrast, our previous result (Blair and Iwasaki (2011)) obtains a globally optimal solution to an approximate model obtained through techniques such as Taylor series and describing function, which works well for systems in constant contact with the environment (such as swimming). The problem is first formulated as the minimization of a quadratic cost function over the set of periodic functions subject to an average velocity constraint, then solved by a generalized eigenvalue computation with a frequency search. This method also ensures that the optimal gait is achievable with the given set of actuators by formulating the problem in terms of the input u.

This paper focuses on bird or fish-like systems which are in constant contact with the surrounding environment and locomote primarily through the periodic motion of wings (or fins), which we call "flapping-wing" rectifiers. These systems are of particular interest for underwater vehicles due to their expected maneuverability, silence, and efficiency. We develop the equations of motion for a simple flapping-wing rectifier, where we assume a simple point-mass model for the wing geometry, and allow independent wing motion and body translation and rotation. We briefly review the optimal gait problem and numerical solution process described in (Blair and Iwasaki (2011)), and apply the optimal gait theory to the flapping-wing rectifier to examine the effects of various wing shapes and optimality criteria on gait selection.

We show that the bilinear thrust term has a strong influence on gait selection by comparing the basic efficient gait (which maximizes the ratio of the thrust to wing deflection) with other optimal gait results through gait snapshot, amplitude, and phase plots. We find that a long, high-aspect-ratio wing results in an oscillatory (flapping) gait while a short, low-aspect-ratio wing results in an undulatory gait. In addition, we observe that the optimal gait which minimizes actuation changes from symmetric with body pitching to anti-symmetric with body rolling as the frequency of oscillation is increased.

⋆ This work is supported by the Office of Naval Research under MURI Grant N00014-08-1-0642, and by the National Science Foundation under No.0654070.

2. FLAPPING-WING MODEL

2.1 Overview

In this section we develop a nonlinear model for simple flapping-wing rectifiers, then approximate the model assuming small displacements using Taylor series to extract the essential dynamics of rectification given by a bilinear equation.

The coordinate system is defined so that, at the nominal condition, the body lies on the (x,y) plane with the y-axis being the direction of swimming and the z-axis being vertical. The model consists of a main body (to which the "wings" attach) featuring full rigid-body rotational and translational dynamics. We define $\phi_b \in \mathbb{R}^3$ as the vector of body orientation variables (Euler angles in the $(z\text{-}y\text{-}x)$ convention describing yaw α_b, roll β_b, and pitch γ_b), and $r_b \in \mathbb{R}^3$ as the Cartesian coordinates of the body in the global frame. Each wing may move independently and is described by the displacement of n discrete point-masses, located at the intersections of a body-fixed Cartesian grid, which can be seen in Fig. 1. The body-fixed Cartesian coordinate system is denoted by (x^b,y^b,z^b), with the position of the i^{th} point-mass in the body frame given by (x_i^b, y_i^b, z_i^b), and the collection of all point-mass positions denoted by $r^b := \text{col}(x^b, y^b, z^b) \in \mathbb{R}^{3n}$ in the body frame and $r := \text{col}(x, y, z) \in \mathbb{R}^{3n}$ in the inertial frame. We fix the point-masses to move in the z^b direction only (i.e. x^b and y^b are constant) and capture wing stiffness and actuation by torques approximated as linear force couples acting in the z^b direction between adjacent point-masses.

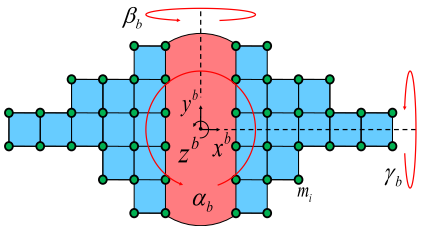

Fig. 1. Flapping-wing system with point-mass wings.

2.2 Equations of motion

The general framework we use to derive the equations of motion is given by the Euler-Lagrange equation:

$$\frac{d}{dt}\left(\frac{\partial L}{\partial \dot{q}}\right) - \frac{\partial L}{\partial q} = \psi, \tag{1}$$

where $q(t) \in \mathbb{R}^{n+6}$ are the generalized coordinates, $\psi(t) \in \mathbb{R}^{n+6}$ are the generalized forces, and $L(q, \dot{q}) := T - V \in \mathbb{R}$ is the difference between the kinetic energy $T(q, \dot{q})$ and the potential energy $V(q)$. We choose $q := \text{col}(\theta, r_t)$, where $\theta := \text{col}(z^b, \phi_b)$ is the shape and orientation of the system and $r_t \in \mathbb{R}^3$ are the Cartesian coordinates of the center of mass of the system.

The kinetic and potential energies are expressed in the generalized coordinates q as

$$\begin{aligned} T &= \frac{1}{2}\left(\dot{r}^\mathsf{T} M \dot{r} + m_b \dot{r}_b^\mathsf{T} \dot{r}_b + \dot{\phi}_b^\mathsf{T} J_{\phi_b}(\phi_b)\dot{\phi}_b\right) \\ &= \begin{bmatrix} \dot{\theta} \\ \dot{r}_t \end{bmatrix}^\mathsf{T} \begin{bmatrix} J(\theta) & 0 \\ 0 & m_t I_3 \end{bmatrix} \begin{bmatrix} \dot{\theta} \\ \dot{r}_t \end{bmatrix}, \\ V &= \frac{1}{2} z^{b\mathsf{T}} K z^b, \end{aligned} \tag{2}$$

where we assumed that the system is neutrally buoyant and thus ignored potential energy due to gravity, and $M := I_3 \otimes \text{diag}(m_i)$ where m_i is the mass of point-mass i, m_b is the mass of the main body, m_t is the mass of the whole system, $J_{\phi_b}(\phi_b) \in \mathbb{R}^{3\times3}$ is the inertia matrix for the main body as a function of orientation, $J(\theta) \in \mathbb{R}^{(n+3)\times(n+3)}$ is the inertia matrix for the whole system as a function of θ, $I_x \in \mathbb{R}^{x\times x}$ is an identity matrix, and $K := T_\tau^\mathsf{T} K_\tau T_\tau$ is the stiffness matrix in the z^b coordinate where K_τ is a torsional joint stiffness and T_τ is a transformation matrix from the z^b coordinates to joint angles.

The generalized forces consist of actuation torques and fluid forces from the environment, and are defined using the principle of virtual work,

$$\delta W = (\delta q)^\mathsf{T} \psi, \tag{3}$$

where δW is a virtual work resulting from a virtual displacement δq acted upon by force ψ. To approximate torques with our simple point-mass model we use linear force couples acting on neighboring point-masses in the z^b direction as shown in Fig. 2. The virtual work due to

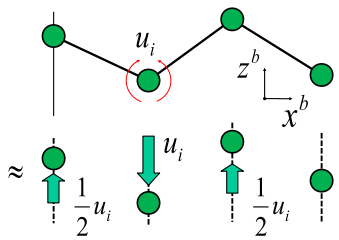

Fig. 2. Torque approximation.

actuation is thus

$$\delta W_a = (\delta q)^\mathsf{T} B(\theta) u, \tag{4}$$

where

$$B(\theta) := \frac{\partial r_o}{\partial q}^\mathsf{T} B_{r_o}(\theta) + \frac{\partial r}{\partial q}^\mathsf{T} B_r(\theta),$$

and r_o are the points on the main body being acted on by the actuators at the first point mass in each row and $B_{r_o}(\theta)$ and $B_r(\theta)$ are matrices mapping the actuation vector u to the vectors of forces acting on the body points and point-masses respectively.

We approximate the forces exerted by the environment on the wings as static functions of the normal and tangential velocity of the wing surface. This type of static force models have been used for undulatory locomotion (Taylor (1952); Saito et al. (2002)). We further make linear approximations of the static force functions to capture, at least qualitatively, the anisotropy property (easier to slide in the tangential direction than in the normal direction) which is known to be important for mechanical rectification. The added mass effect, which could also be important, is not captured by the current model.

At each mass, the plane normal to the wing surface is determined from the coordinates of the surrounding

masses, as shown in Fig. 3. The velocity vector for each

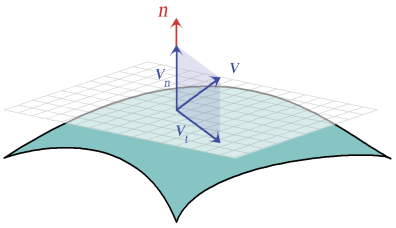

Fig. 3. Surface normal and velocity projections.

mass is projected into the normal and tangential directions and then multiplied by the normal and tangential coefficient to obtain the fluid force acting on each mass in the normal and tangential directions, respectively. The virtual work due to the environmental fluid force is thus

$$\begin{aligned} \delta W_e &= (\delta q)^{\mathsf{T}} \left(\frac{\partial r}{\partial q}\right)^{\mathsf{T}} f, \quad f := f_n + f_t, \\ f_n &:= -C_n v_n, \qquad f_t := -C_t v_t \\ v_n &:= R_{\phi_b}^{\mathsf{T}} P_n^b R_{\phi_b} \dot{r}, \qquad v_t := R_{\phi_b}^{\mathsf{T}} \left(I_{3n} - P_n^b\right) R_{\phi_b} \dot{r}, \end{aligned} \tag{5}$$

where $f \in \mathbb{R}^{3n}$ is the vector of (x, y, z) force components acting on the n point-masses, $f_n \in \mathbb{R}^{3n}$ and $f_t \in \mathbb{R}^{3n}$ are the normal and tangential environmental force components, respectively, $v_n \in \mathbb{R}^{3n}$ and $v_t \in \mathbb{R}^{3n}$ are the normal and tangential velocities of the point-masses, $C_n := I_3 \otimes \mathrm{diag}(c_{n_i})$ and $C_t := I_3 \otimes \mathrm{diag}(c_{t_i})$ are the fluid force coefficient matrices where c_{n_i} and c_{t_i} are the normal and tangential coefficients for point-mass i, $P_n^b \in \mathbb{R}^{3n \times 3n}$ is the surface normal projection matrix in the body frame (for every point-mass), and $R_{\phi_b} \in \mathbb{R}^{3n \times 3n}$ is the rotation matrix relating the inertial frame to the body frame (for every point-mass).

Gathering the terms, we obtain the nonlinear equations of motion given by

$$\begin{aligned} \begin{bmatrix} J(\theta) & 0 \\ 0 & m_t I_3 \end{bmatrix} \begin{bmatrix} \ddot{\theta} \\ \ddot{r}_t \end{bmatrix} + \begin{bmatrix} G(\theta, \dot{\theta})\dot{\theta} \\ 0 \end{bmatrix} + \begin{bmatrix} \mathcal{K}\theta \\ 0 \end{bmatrix} \\ - \left(\frac{\partial r}{\partial q}\right)^{\mathsf{T}} f = B(\theta) u, \end{aligned} \tag{6}$$

where

$$\mathcal{K} = \begin{bmatrix} K & 0 \\ 0 & 0 \end{bmatrix}, \quad G(\theta, \dot{\theta}) := \frac{\partial J(\theta)\dot{\theta}}{\partial \theta} - \left(\frac{\partial J(\theta)\dot{\theta}}{\partial \theta}\right)^{\mathsf{T}}.$$

The rows corresponding to $\ddot{\theta}$ and $\ddot{r}_t$ are termed the "shape dynamics equation" and "rectifier equation", respectively, and this is a specific case of the general equations of motion for mechanical rectifiers developed in (Blair and Iwasaki (2011)).

Assuming small displacements and small rotations, we use the Taylor series expansion to obtain the simplest model which contains the essential dynamics of rectification. Reference (Blair and Iwasaki (2011)) shows that a fully linear approximation fails to capture the rectifying dynamics; a bilinear term of θ and $\dot{\theta}$ in the rectifier equation is needed. Keeping terms up to the first order in θ in the shape dynamics equation and up to the second order in θ in the rectifier equation, we obtain the bilinear equations of motion given by

$$\begin{bmatrix} J(0)\ddot{\theta} + \mathcal{K}\theta \\ m_t \ddot{r}_t \end{bmatrix} + \begin{bmatrix} D & L(\theta) \\ L(\theta)^{\mathsf{T}} & Q(\theta) \end{bmatrix} \begin{bmatrix} \dot{\theta} \\ \dot{r}_t \end{bmatrix} = \begin{bmatrix} B \\ 0 \end{bmatrix} u, \tag{7}$$

where $L(\theta)$ is affine in θ and $Q(\theta)$ is quadratic in θ.

2.3 Model parameters

The fluid forces are approximated based on theory by Taylor (1952), adjusted for undulator swimming by Chen et al. (2011), with separate coefficients for the tangential and normal directions. The wing and body dimensions are arbitrarily chosen to be reasonable for a small unmanned robot. We examine three systems, a high-aspect-ratio and low-aspect-ratio rectangular wing and a triangular wing. The wing and body density is approximated as the density of water.

The nominal model parameters are given by

	High-aspect	Low-aspect	Triangular
ℓ_w	0.14 m	0.08 m	0.2 m
ℓ_b	0.14 m	0.26 m	0.2 m

$c_{n_i} = \frac{3\rho v_o d^2}{2}$ Ns/m $\quad c_{t_i} = \frac{2.7dx\sqrt{\rho\mu d v_o a_i}}{2}$ Ns/m
$a_b = \frac{0.03\rho v_y A_b}{2}$ Ns/m $\quad m_i = \rho d^2 t_w$ kg
$\rho = 1000$ kg/m^3 $\quad \mu = 10^{-3}$ Ns/m^2
$d = 0.01$ m $\quad A_b = 0.012$ m^2 $\quad v_o = 0.1$ m/s
$t_w = 0.01$ m $\quad w_b = 0.06$ m $\quad v_y = 2\ell_b$ m/s

where ℓ_w is the body-to-tip span of one wing, ℓ_b is the body length, c_{n_i} and c_{t_i} is the normal and tangential coefficient of friction for point mass i, a_b is the drag coefficient for the main body, m_i is the mass of point mass i, ρ is the density of water, μ is the viscosity of water, d is the distance between point masses, A_b is the main body area, v_o is the approximate operating region for the normal wing velocity, t_w is the wing thickness, w_b is the body width, and v_y is the average steady-state velocity.

3. FLAPPING GAIT ANALYSIS

3.1 Review of the optimal gait theory

A brief summary of the basic gait and optimal gait problem formulations and solutions as shown in (Blair and Iwasaki (2011)) follows.

The rectifier equation in (7) shows that a periodic motion θ leads to the thrust $-L(\theta)^{\mathsf{T}}\dot{\theta}$ and drag $Q(\theta)\dot{r}_t$. To consider the thrust in the direction of locomotion y, let us define a constant matrix Λ such that $L(\theta)e_2 = \Lambda\theta$, where $e_2 := \mathrm{col}(0, 1, 0)$. From the thrust term we see that the essential dynamics of rectification is captured by the skew-symmetric part of the linear coefficient matrix in $L(\theta)$, since the average thrust α over one period T is

$$\alpha = -\int_0^T (\Lambda\theta)^{\mathsf{T}}\dot{\theta}dt = -\int_0^T \dot{\theta}^{\mathsf{T}} S\theta dt, \quad S := \frac{\Lambda - \Lambda^{\mathsf{T}}}{2}.$$

This shows that the bilinear equations of motion are the lowest order approximate system capable of capturing the essential thrust terms for locomotion; if the equations of motion were fully linearized, $\Lambda = 0$ and the thrust is lost. In fact, the basic mechanism for gait selection is embedded in the eigenvectors of S.

The eigenvector θ_o associated with the maximum real eigenvalue λ_o satisfying $(jS - \lambda_o Y)\theta_o = 0$ gives the basic gait which maximizes the thrust to amplitude ratio at a given cycle frequency ω:

$$\max_{\theta \in \mathbb{P}_T} \frac{\int_0^T (-\dot{\theta}^\mathsf{T} S \theta) dt}{\int_0^T \|\varphi\|^2 dt} = \max_{\hat{\theta} \in \mathbb{C}^n} \frac{j\omega \hat{\theta}^* S \hat{\theta}}{\hat{\theta}^* Y \hat{\theta}} = \omega \lambda_o, \tag{8}$$

where $\mathbb{P}_T$ is the set of T-periodic, continuously differentiable, unbiased signals, $\varphi := Y^{1/2}\theta$ is some measure of amplitude expressed as a linear function of θ (such as displacement, angle, or curvature), $T := 2\pi/\omega$, and the global maximum is attained by a harmonic gait at $\hat{\theta} = \theta_o$ or $\theta(t) = \Re[\theta_o e^{j\omega t}]$. Optimal gaits with respect to additional criteria are variations of the basic gait embedded in the bilinear rectification mechanism.

We formulate the optimal gait problem as the minimization of a quadratic cost function subject to an average velocity constraint over one period of oscillation, given by

$$\begin{aligned} \min_{\substack{T \in \mathbb{R}_+ \\ v, \theta, u \in \mathbb{P}_T}} \quad & \frac{1}{T}\int_0^T \begin{bmatrix} \theta \\ u \end{bmatrix}^\mathsf{T} \mathring{\Pi} \begin{bmatrix} \theta \\ u \end{bmatrix} dt \quad \text{subject to} \\ & \frac{1}{T}\int_0^T \dot{r}_t dt = \begin{bmatrix} 0 \\ v_y \\ 0 \end{bmatrix}, \end{aligned} \tag{9}$$

where $\Pi(s) \in \mathbb{\Pi}$ is a given transfer function, with $\mathbb{\Pi}$ being the set of transfer functions of the form $\Pi(s) = F(-s)^\mathsf{T} \Psi F(s)$, where Ψ is a constant Hermitian matrix and $F(s)$ is a linear combination of stable (proper) transfer functions and differentiators. We denote the T-periodic signal $y^\mathsf{T}\Psi y$ by $\mu^\mathsf{T}\mathring{\Pi}\mu$, where y is the steady state response to input $\mu \in \mathbb{P}_T$.

For tractability, we further approximate the equations of motion as

$$\begin{aligned} & J(0)\ddot{\theta} + D\dot{\theta} + (\mathcal{K} + v_y \Lambda)\,\theta = Bu, \\ & m_t \dot{v}_y + (a_y + \theta^\mathsf{T} Q_y \theta) v_y + \theta^\mathsf{T} \Lambda^\mathsf{T} \dot{\theta} = 0, \end{aligned} \tag{10}$$

where we choose the direction of motion to be in the y direction, set $\dot{r}_t = \mathrm{col}(0, v_y, 0)$ in the shape equation, and ignore the dynamics of r_{t_x} and r_{t_z} in the rectifier equation under the argument that acceleration in those directions will naturally be eliminated during the optimization process. The problem is then reformulated by substituting (10) into (9) while averaging over one cycle, yielding a new problem given by

$$\begin{aligned} \min_{\substack{T \in \mathbb{R}_+ \\ v, \theta, u \in \mathbb{P}_T}} \quad & \frac{1}{T}\int_0^T \begin{bmatrix} \theta \\ u \end{bmatrix}^\mathsf{T} \mathring{\Pi} \begin{bmatrix} \theta \\ u \end{bmatrix} dt \quad \text{subject to} \\ & \int_0^T \Big((a_y + \theta^\mathsf{T} Q_y \theta) v_y + \dot{\theta}^\mathsf{T} \Lambda \theta \Big)\, dt = 0, \\ & J(0)\ddot{\theta} + D\dot{\theta} + (\mathcal{K} + v_y \Lambda)\,\theta = Bu. \end{aligned} \tag{11}$$

The solution to this problem is then given by Theorem 1.

Theorem 1. (Blair and Iwasaki (2011)). *Consider the optimal locomotion problem given by (11). Define $X(\omega)$ and $Y(\omega)$ as*

$$\begin{aligned} X(\omega) &:= \frac{1}{2}\begin{bmatrix} P(\omega) \\ I \end{bmatrix}^* \Pi(j\omega) \begin{bmatrix} P(\omega) \\ I \end{bmatrix}, \\ Y(\omega) &:= P(\omega)^* (S(\omega) - v_y Q_y) P(\omega) / (2 a_y v_y), \\ S(\omega) &:= j\omega(\Lambda - \Lambda^\mathsf{T})/2, \\ P(\omega) &:= (v_y \Lambda + \mathcal{K} + j\omega D - \omega^2 J(0))^{-1} B. \end{aligned}$$

Let γ be the optimal value of the objective function. Then we have

$$\gamma = \min_{\omega \in \mathbb{R}} \max_{\lambda \in \mathbb{R}} \ \{\, \lambda : \ X(\omega) \geq \lambda Y(\omega) \,\}. \tag{12}$$

Let ω_o and λ_o be the optimizers. Then, the optimal period is $T = 2\pi/\omega_o$, and the optimal gait ϑ and input u are given by

$$u(t) = \Re[z_o e^{j\omega_o t}], \quad \vartheta(t) = \Re[P(\omega_o) z_o e^{j\omega_o t}],$$

where $z_o \in \mathbb{C}^\ell$ is the eigenvector of the pair $(X(\omega_o), Y(\omega_o))$ associated with the generalized eigenvalue λ_o, normalized to satisfy $z_o^* Y(\omega_o) z_o = 1$.

3.2 Effects of wing geometry on basic flapping gaits

In this section we examine the effect of wing aspect ratio on the basic gait for simple flapping-wing rectifiers. We examine a single wing with the body fixed to translate only in the y-direction with no rotation, and we apply (8) with φ chosen to be a form of the wing curvature by setting

$$Y := \begin{bmatrix} T_c^\mathsf{T} T_c & 0 \\ 0 & 0 \end{bmatrix},$$

where $\mathrm{col}(c_x, c_y) := T_c z^b$ are the wing curvatures in the x^b and y^b directions at each point mass, and T_c is the associated transformation matrix.

Figure 4 shows four snapshots of the basic gait for the high aspect ratio case, where plots (a) to (d) correspond to equally spaced time instants $t = 0$ to $3T/4$. The wing is connected to the body along the lower-left edge (parallel with the y-axis) and the system locomotes in the positive y direction. Figure 5 shows the associated amplitude and phase contours.

Similarly, Figs. 6 and 7 show the basic gait snapshots and amplitude and phase plots for the low aspect ratio case. The contour colors are consistent through all contour plots and are shown in Fig.7, with units of meters for amplitude and 2π radians for the phase (i.e. a phase of 0.5 corresponds to π radians).

In the high aspect ratio plots we see a flapping gait with a relatively small number of waves down the wing. The amplitude of wing defection smoothly increases away from the body in a roughly radial manner and a traveling wave progresses from head to tail in a straight fashion. In the low aspect ratio plots we see a more undulatory gait with a larger number of waves down the wing. The general shapes of the amplitude and phase contours are similar between the two cases. We thus observe that a short, low-aspect-ratio wing tends to undulate while a long, high-aspect-ratio wing tends to flap.

3.3 Optimal Gaits

We now examine the optimal gait by solving (11) where we minimize the norm squared of the actuation vector, u, subject to the average velocity constraint. We examine a system with high aspect ratio triangular shaped wings, which are allowed to move independently, while the body is free to translate and rotate in any direction. We examine two oscillation frequencies, 4 and 8 radians per second, which approximately correspond to the first and second natural modes.

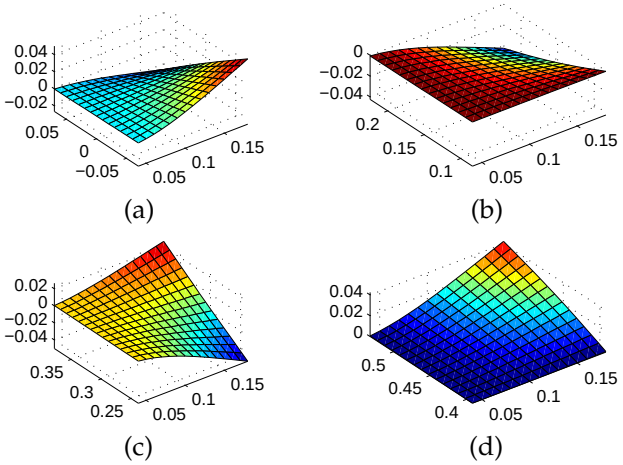

Fig. 4. High-aspect basic gait snapshots

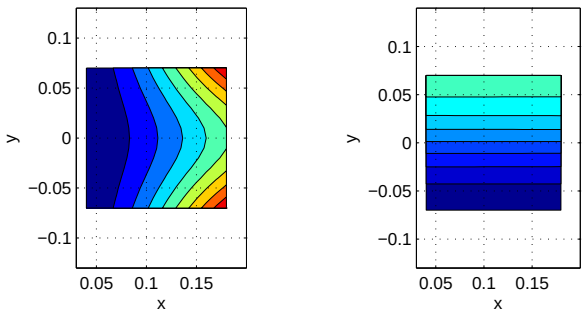

Fig. 5. High-aspect basic gait amplitude and phase

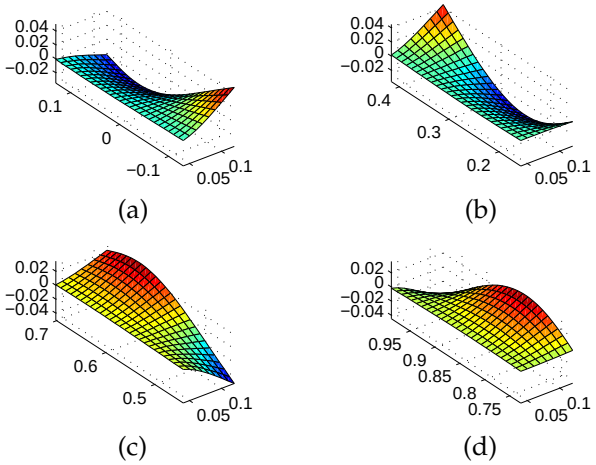

Fig. 6. Low-aspect basic gait snapshots

Figure 8 shows four snapshots of the optimal gait for $\omega = 4$, where plots (a) to (d) correspond to equally spaced time instants $t = 0$ to $3T/4$, and Fig. 9 shows the optimal amplitude and phase. All plots are in the body frame. The optimal gait is a symmetric oscillatory (or flapping) motion with some slight body pitching (not shown), due to the heaving motion of the wings. Rolling is not observed due to the symmetric gait. The general shape of the phases and amplitudes are similar to the basic gait results, with a phase lag (or wave) propagating from head to tail along each wing in an almost straight fashion.

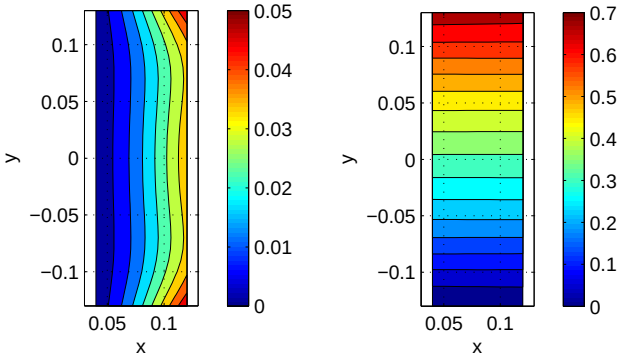

Fig. 7. Low-aspect basic gait amplitude and phase

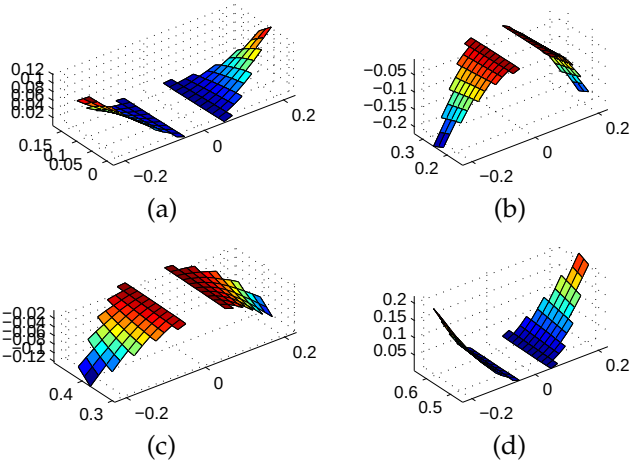

Fig. 8. Optimal gait snapshots, $\omega = 4$

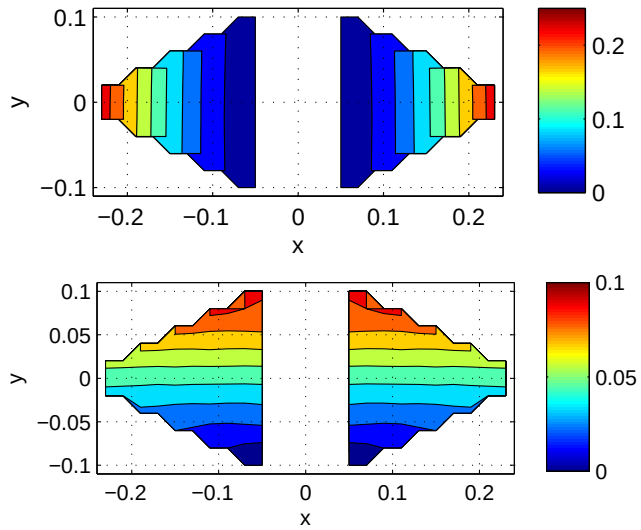

Fig. 9. Optimal gait amplitude and phases, $\omega = 4$

Similarly, Figs. 10 and 11 show the optimal gait snapshots and amplitude and phase plots for the same system, however with a doubled oscillation frequency. Interestingly, the resulting optimal gait is now anti-symmetric with body rolling but no body pitching. The general shape of the amplitudes are similar to the previous case, however the phases are different. Counter intuitively, near the body the phases indicate a wave running counter to

the direction of thrust, while at the wing tips, the proper phase lag is observed for thrust generation. This occurs because the actuation is exciting the second natural mode of the system by taking advantage of the stiffness in the wing, which results in an out-of-phase relationship between the base of the wing and the wing tip. Any backward thrust generated by this motion is negligible due to the very small amplitudes compared to the wing tip.

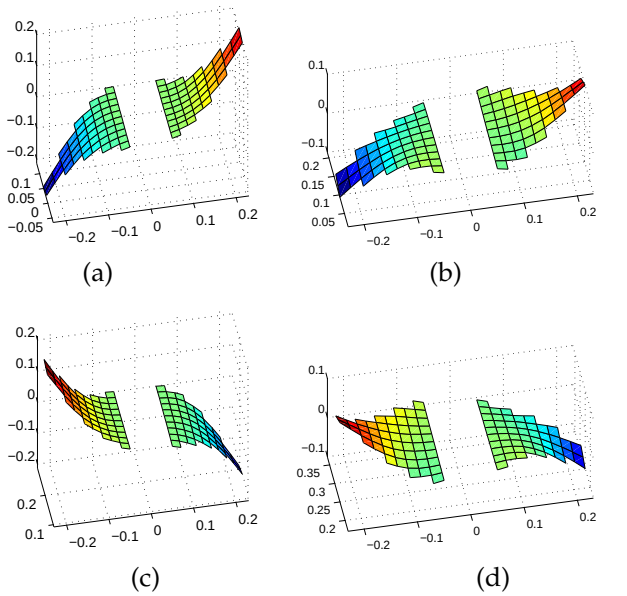

Fig. 10. Optimal gait snapshots, $\omega = 8$

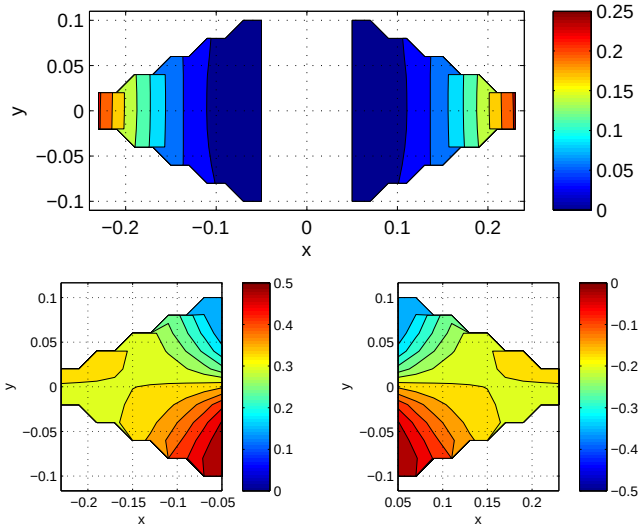

Fig. 11. Optimal gait amplitude and phases, $\omega = 8$

These results indicate a general trend where the wing amplitude contour is primarily determined by the specific shape of the wing through S in the basic gait calculation, while the phase contour depends on the natural modes. Straight phase lags correspond to the symmetric first natural mode and agree with the basic gait calculation, while more complicated phase lags correspond to the antisymmetric second natural mode.

4. CONCLUSION

We have examined the basic and optimal gaits for simple flapping-wing rectifiers with varying wing geometries. For the basic gait analysis we examined a single wing with the body fixed to translate only in the y-direction with no rotation, and saw that as the aspect ratio of the wing changed from high to low, the underlying basic gait changed from oscillation to undulation. For the optimal gait analysis we examined a system with two independent wings with the body free to translate and rotate in any direction, and saw similar amplitude contours with the basic gait results. In addition, we also observed that the optimal gait changed from a symmetric gait with body pitching (and no rolling) to an anti-symmetric gait with body rolling (and no pitching) as the oscillation frequency is increased. These results are interesting as they indicate that there is a relationship between body geometry, frequency, locomotion speed, and optimal gait where passing a critical threshold results in a sudden transition from symmetric pitching to anti-symmetric rolling through utilization of a different natural mode.

REFERENCES

Bessonnet, G., Chesse, S., and Sardain, P. (2004). Optimal gait synthesis of a seven-link planar biped. *The International journal of robotics research*, 23(10-11), 1059–1073.

Blair, J. and Iwasaki, T. (2011). Optimal gaits for mechanical rectifier systems. *IEEE Trans. Auto. Contr.*, 56(1), 59–71.

Chen, J., Friesen, W., and Iwasaki, T. (2011). Mechanisms underlying rhythmic locomotion: Body-fluid interaction in undulatory swimming. *J. Exp. Biol.*, 214(4), 561–574.

Chevallereau, C. and Aoustin, Y. (2001). Optimal reference trajectories for walking and running of a biped robot. *Robotica*, 19, 557–569.

Cortes, J., Martinez, S., Ostrowski, J., and McIsaac, K. (2001). Optimal gaits for dynamic robotic locomotion. *The International journal of robotics research*, 20(9), 707–728.

Hicks, G. and Ito, K. (2005). A method for determination of optimal gaits with application to a snake-like serial-link structure. *IEEE Trans. Auto. Contr.*, 50(9), 1291–1306.

McIsaac, K. and Ostrowski, J. (2003). Motion planning for anguilliform locomotion. *IEEE Trans. Robotics and Automation*, 19(4), 637–652.

Ostrowski, J., Desai, J., and Kumar, V. (2000). Optimal gait selection for nonholonomic locomotion systems. *The International journal of robotics research*, 19, 225–237.

Saidouni, T. and Bessonnet, G. (2003). Generating globally optimised sagittal gait cycles of a biped robot. *Robotica*, 21(2).

Saito, M., Fukaya, M., and Iwasaki, T. (2002). Serpentine locomotion with robotic snake. *IEEE Control Systems Magazine*, 22(1), 64–81.

Srinivasan, M. and Ruina, A. (2006). Computer optimization of a minimal biped model discovers walking and running. *Nature*, 439(7072), 73–75.

Taylor, G. (1952). Analysis of the swimming of long and narrow animals. *Proc. Royal Society of London. Series A*, 214(1117), 158–183.